Supporting Information: Self-Consistent Scheme Combining MD and Order-N DFT Methods: An Improved Set of Nonpolarizable Force Fields for Ionic Liquids

Yoshiki Ishii[*,†] and Nobuyuki Matubayasi[*,†,‡]

†*Division of Chemical Engineering, Graduate School of Engineering Science, Osaka University, Toyonaka, Osaka 560-8531, Japan*

‡ *Elements Strategy Initiative for Catalysts and Batteries, Kyoto University, Katsura, Kyoto 615-8520, Japan*

E-mail: y.ishii@cheng.es.osaka-u.ac.jp; nobuyuki@cheng.es.osaka-u.ac.jp

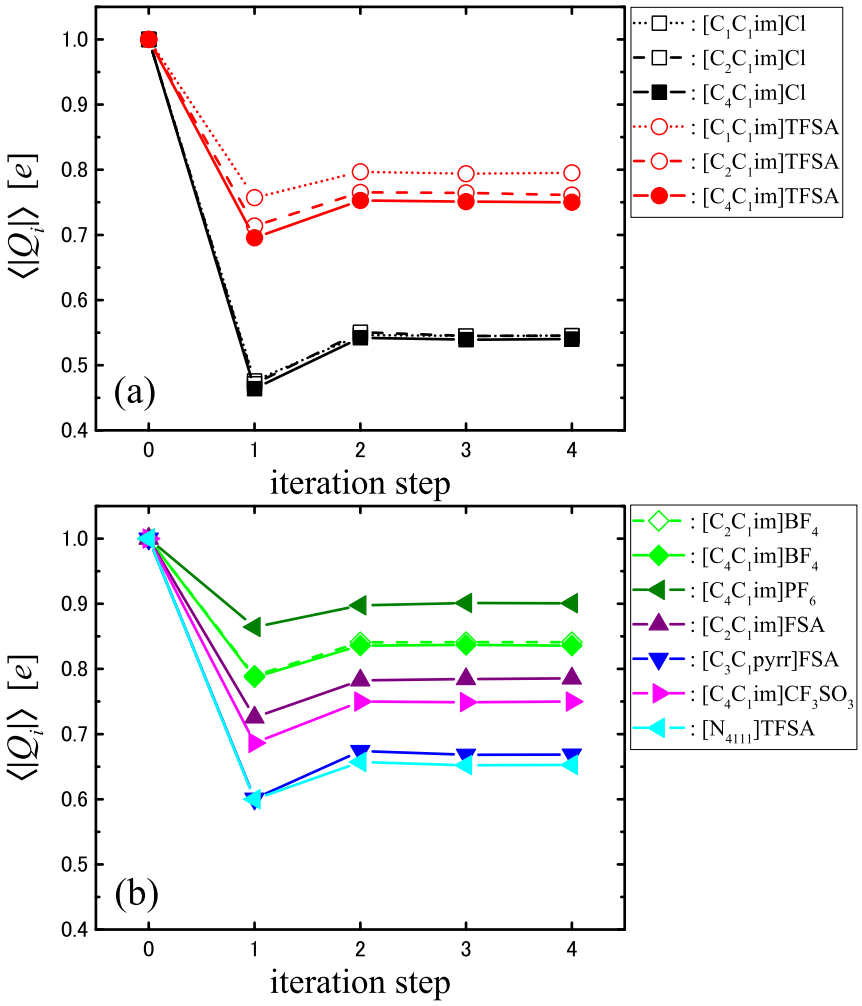

Figure S1: Convergence of DFT-based molecular charges through the self-consistent scheme (a) in $[C_1C_1im]Cl$, $[C_2C_1im]Cl$, $[C_4C_1im]Cl$, $[C_1C_1im]TFSA$, $[C_2C_1im]TFSA$, and $[C_4C_1im]TFSA$, and (b) in $[C_2C_1im]BF_4$, $[C_4C_1im]BF_4$, $[C_4C_1im]PF_6$, $[C_2C_1im]FSA$, $[C_3C_1pyrr]FSA$, $[C_4C_1im]CF_3SO_3$, and $[N_{4111}]TFSA$. The DFT charge is averaged over the 40 cations and 40 anions in the system and the 50 snapshot configurations obtained at the reference state listed in Table 1 with the NVT ensemble.

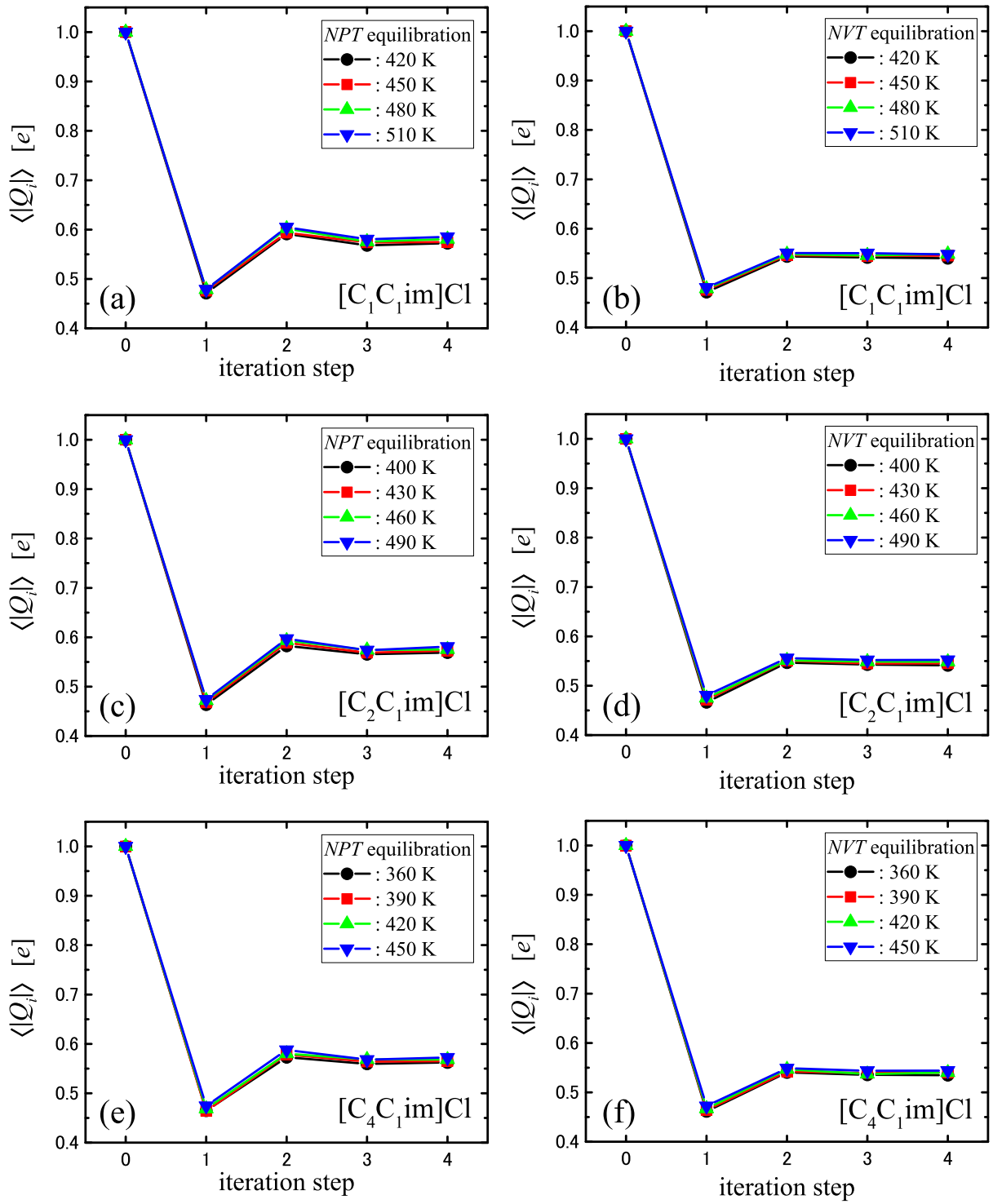

Figure S2: Convergence of DFT-based molecular charges through the self-consistent scheme at all the thermodynamic conditions listed in Table 1 (a,b) in $[C_1C_1im]Cl$, (c,d) in $[C_2C_1im]Cl$, (e,f) in $[C_4C_1im]Cl$, (g,h) in $[C_2C_1im]BF_4$, (i,j) in $[C_4C_1im]BF_4$, (k,l) in $[C_4C_1im]PF_6$, (m,n) in $[C_1C_1im]TFSA$, (o,p) in $[C_2C_1im]TFSA$, and (q,r) in $[C_4C_1im]TFSA$ (s,t) in $[C_2C_1im]FSA$, (u,v) in $[C_3C_1pyrr]FSA$, (w,x) in $[C_4C_1im]CF_3SO_3$, and (y,z) in $[N_{4111}]TFSA$ with the NPT and NVT ensembles, respectively. The DFT charge is averaged over the 40 cations and 40 anions in the system and the 50 snapshot configurations.

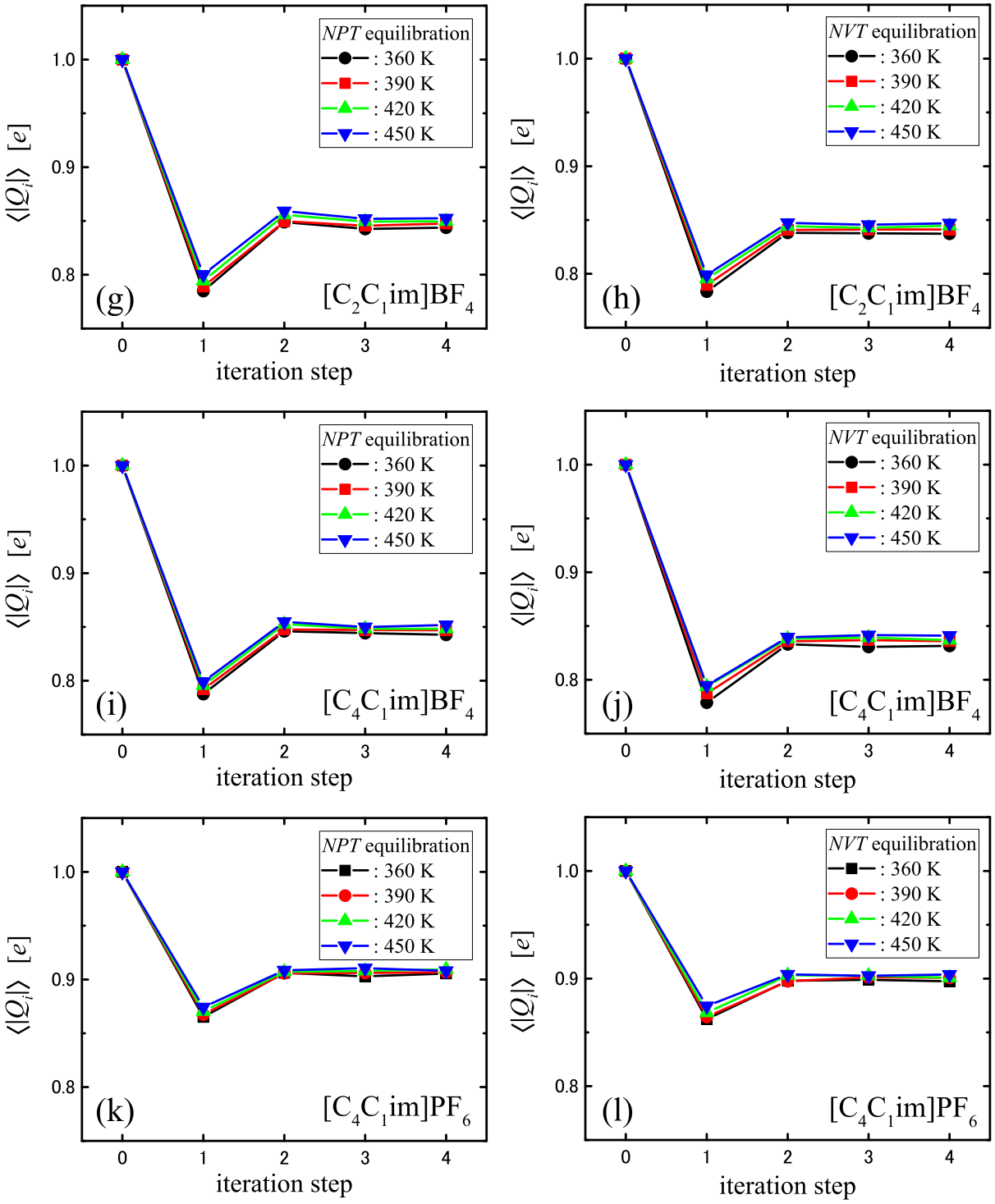

Figure S2: (continued)

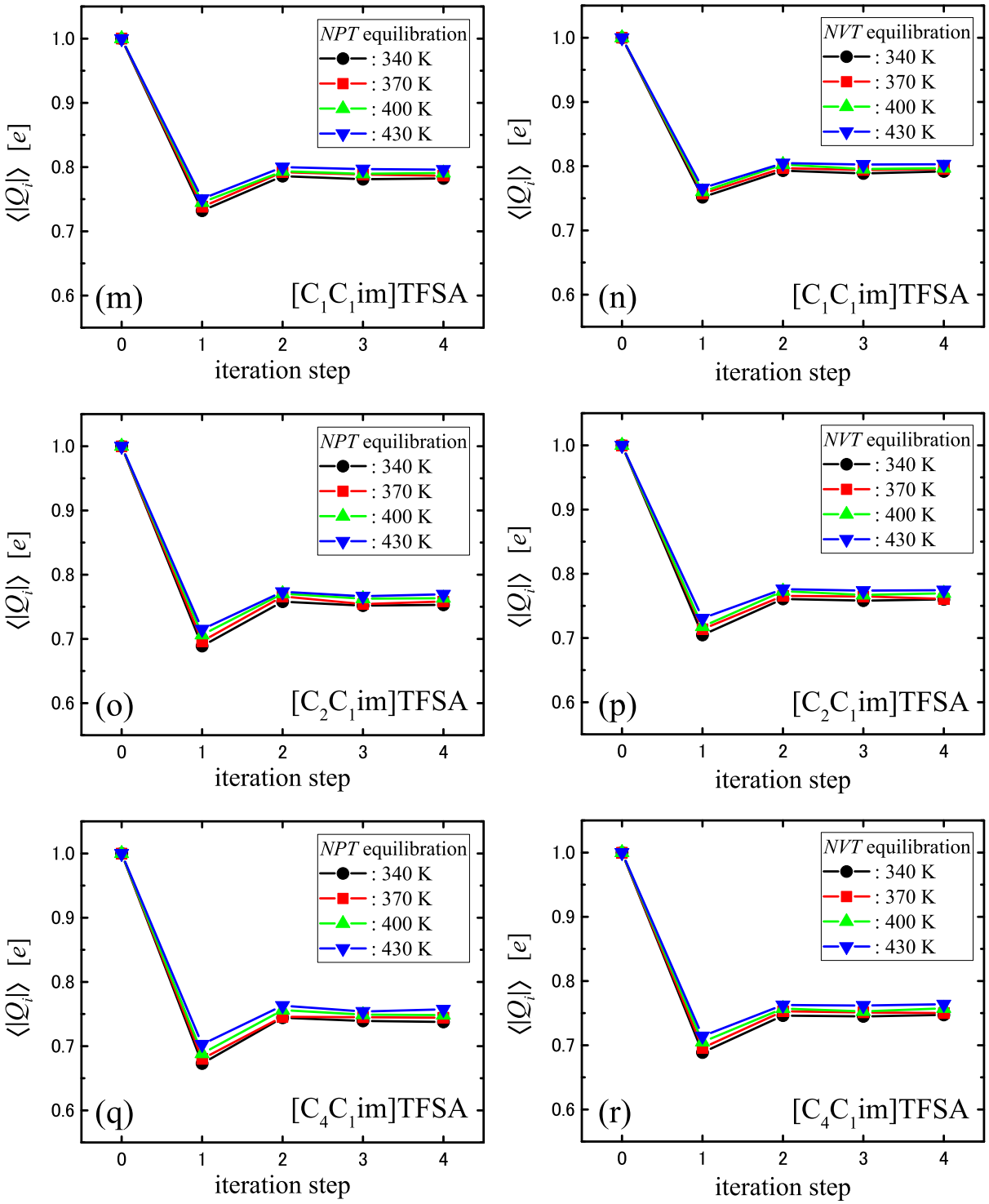

Figure S2: (continued)

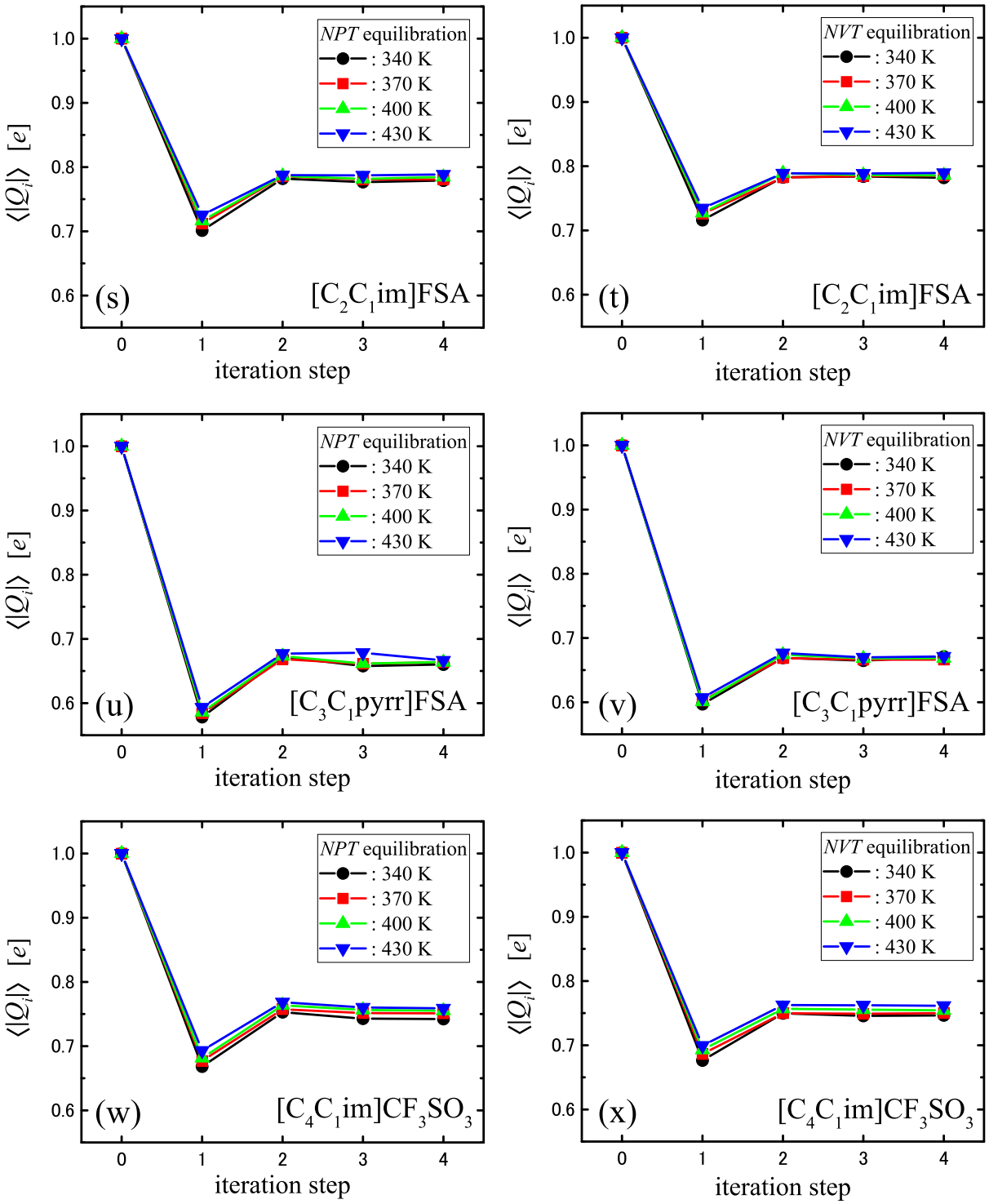

Figure S2: (continued)

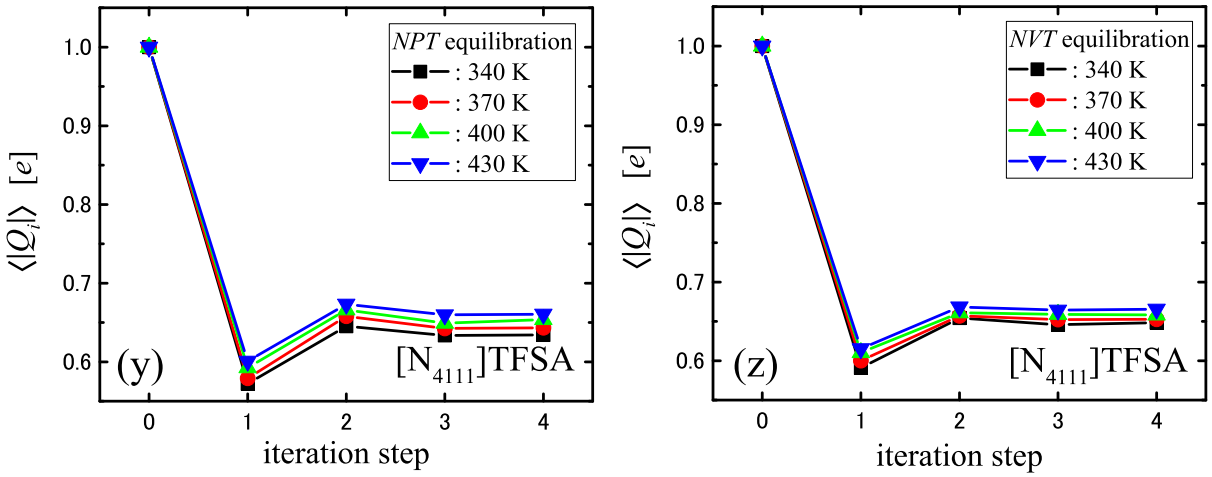

Figure S2: (continued)

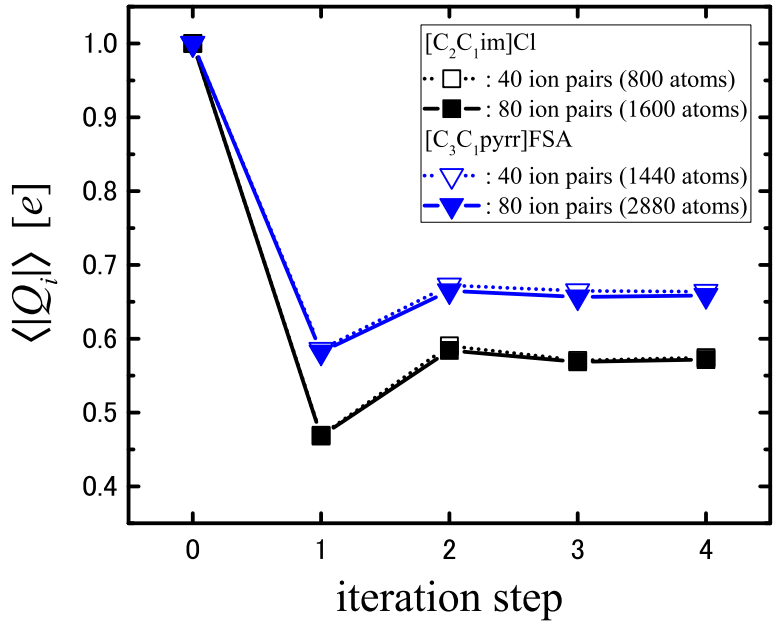

Figure S3: System-size dependence of the convergence of DFT-based molecular charges through the self-consistent scheme in $[C_2C_1im]Cl$ and $[C_3C_1pyrr]FSA$. The DFT charges in the smaller and larger systems are averaged over the 40 cations and 40 anions and over the 80 cations and 80 anions, respectively, at the reference state listed in Table 1 with the NPT ensemble. The 50 snapshot configurations are used for the average in both cases.

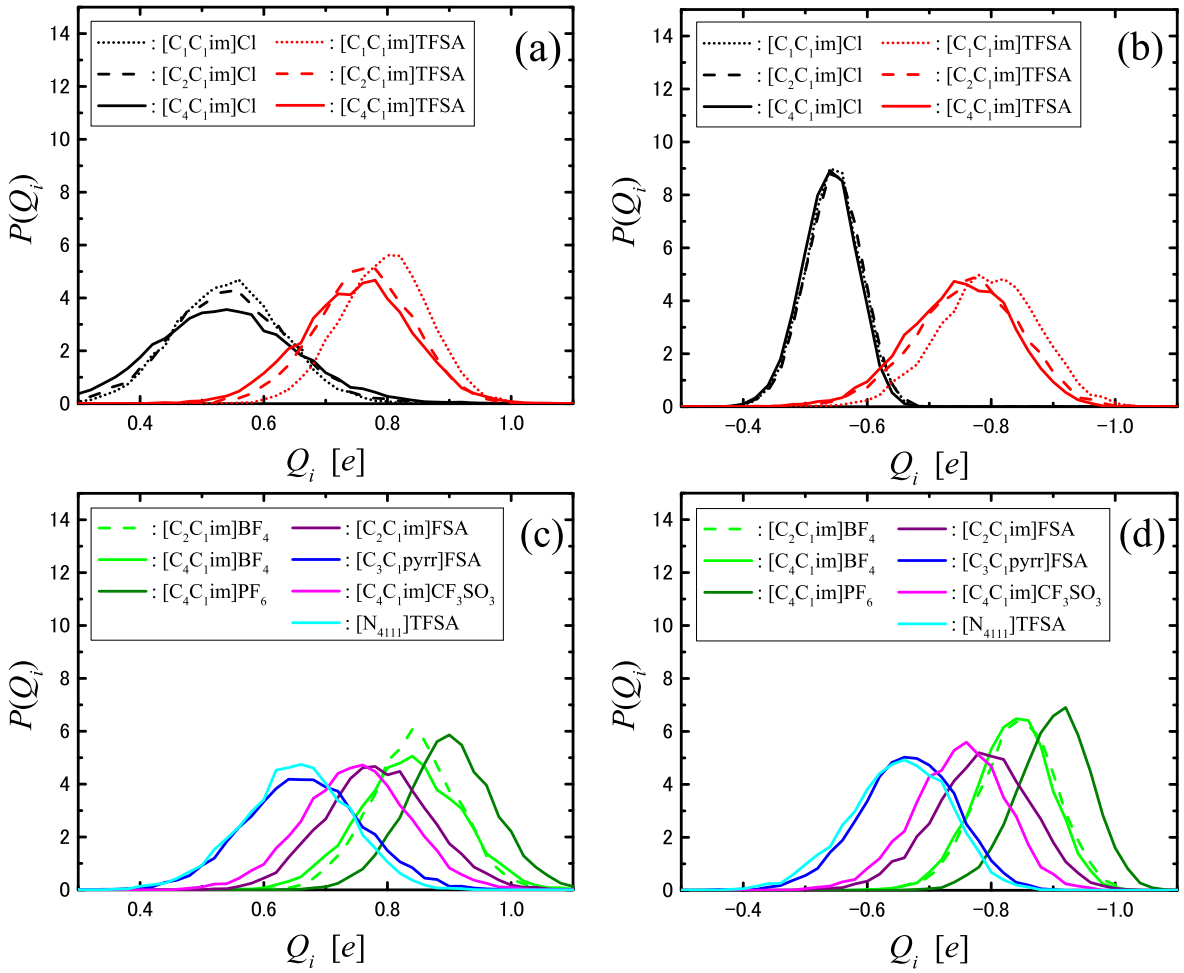

Figure S4: Histrogram of DFT-based molecular charges obtained at the final step of the self-consistent scheme for (a) cations and (b) anions in $[C_1C_1im]Cl$, $[C_2C_1im]Cl$, $[C_4C_1im]Cl$, $[C_1C_1im]TFSA$, $[C_2C_1im]TFSA$, and $[C_4C_1im]TFSA$ and for (c) cations and (b) anions in $[C_2C_1im]BF_4$, $[C_4C_1im]BF_4$, $[C_4C_1im]PF_6$, $[C_2C_1im]FSA$, $[C_3C_1pyrr]FSA$, $[C_4C_1im]CF_3SO_3$, and $[N_{4111}]TFSA$. The DFT charge is averaged with the 200 configurations obtained at the reference state listed in Table 1 with the NVT ensemble.

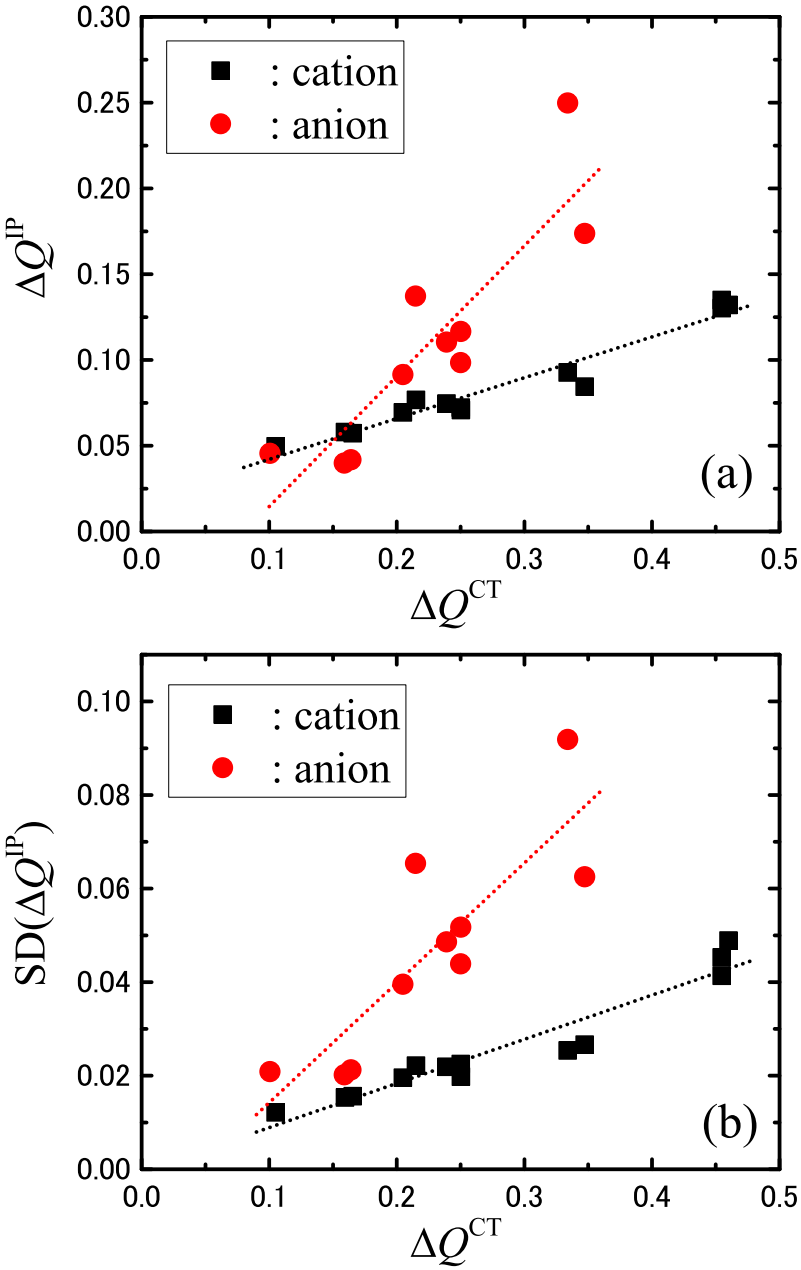

Figure S5: Correlation relationship between the effects of charge transfer and intramolecular polarization for the DFT charges obtained at the final step of the self-consistent scheme in the investigated ionic liquids: (a) ΔQ^{CT} vs ΔQ^{IP}, and (b) ΔQ^{CT} vs $\mathrm{SD}(\Delta Q^{\mathrm{IP}})$. The DFT charge is averaged with the 50 configurations obtained at the reference state listed in Table 1 with the NVT ensemble. With the linear regression against ΔQ^{CT}, the slopes of ΔQ^{IP} are 0.24 and 0.76 for cation and anion, respectively, with correlation coefficients of 0.97 and 0.89, and the slopes of $\mathrm{SD}(\Delta Q^{\mathrm{IP}})$ are 0.09 and 0.26 for cation and anion, respectively, with correlation coefficients of 0.96 and 0.85.

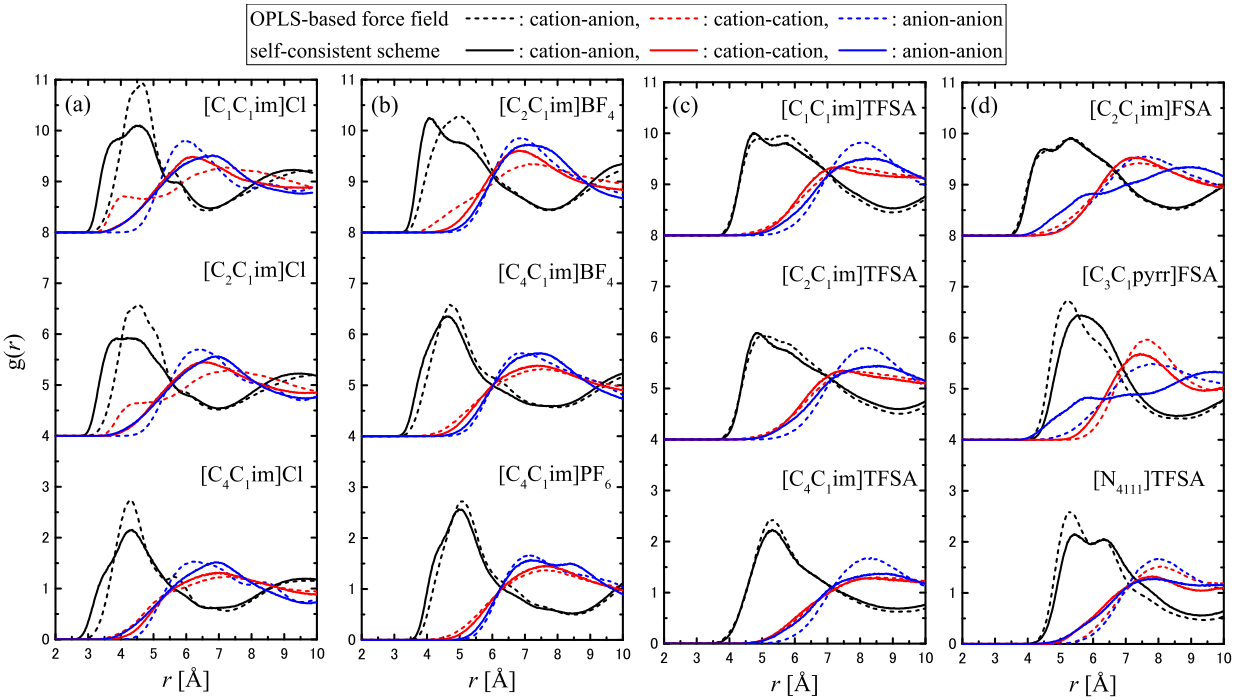

Figure S6: Radial distribution fuctions g(r) between the center-of-masses of cation-anion, cation-cation, and anion-anion (a) in [C_1C_1im]Cl, [C_2C_1im]Cl, and [C_4C_1im]Cl, (b) in [C_2C_1im]BF_4, [C_4C_1im]BF_4, and [C_4C_1im]PF_6, (c) in [C_1C_1im]TFSA, [C_2C_1im]TFSA, and [C_4C_1im]TFSA, and (d) in [C_2C_1im]FSA, [C_3C_1pyrr]FSA, and [N_{4111}]TFSA. They are obtained within the framework of the OPLS-based force field (initial iteration step) and the self-consistent scheme (final iteration step). The upper g(r) values are vertically shifted with an interval of 4 or 8. All the data are obtained at the reference state listed in Table 1 with the NVT ensemble.

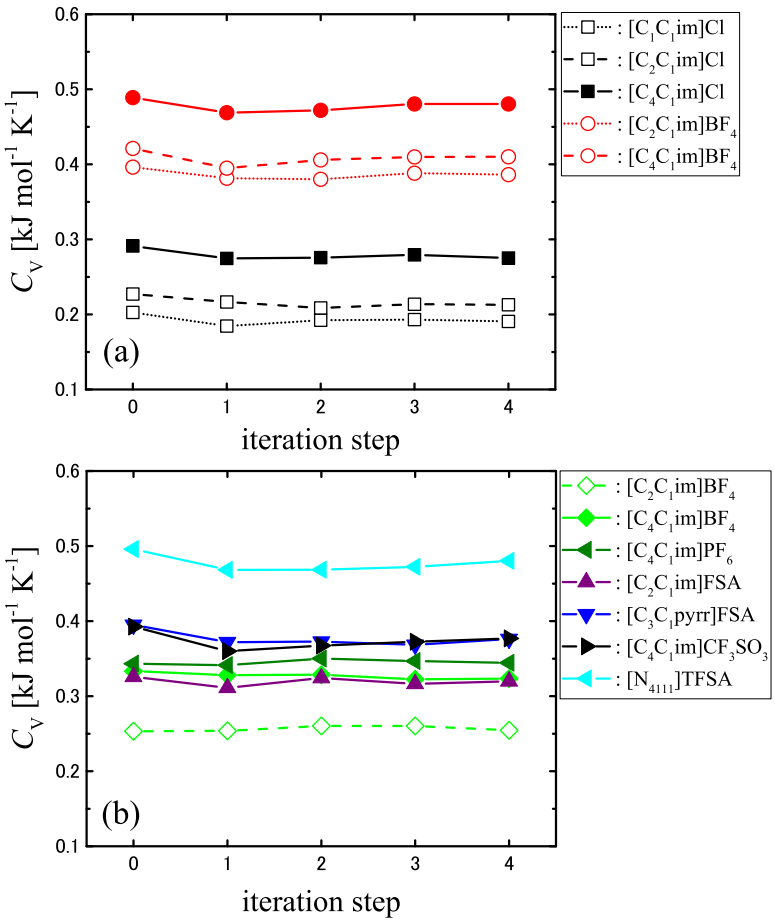

Figure S7: Convergence of heat capacity under constant volume through the self-consistent scheme (a) in [C_1C_1im]Cl, [C_2C_1im]Cl, [C_4C_1im]Cl, [C_1C_1im]TFSA, [C_2C_1im]TFSA, and [C_4C_1im]TFSA and (b) in [C_2C_1im]BF_4, [C_4C_1im]BF_4, [C_4C_1im]PF_6, [C_2C_1im]FSA, [C_3C_1pyrr]FSA, [C_4C_1im]CF_3SO_3, and [N_{4111}]TFSA. All the data are obtained at the reference state listed in Table 1 with NVT ensemble.

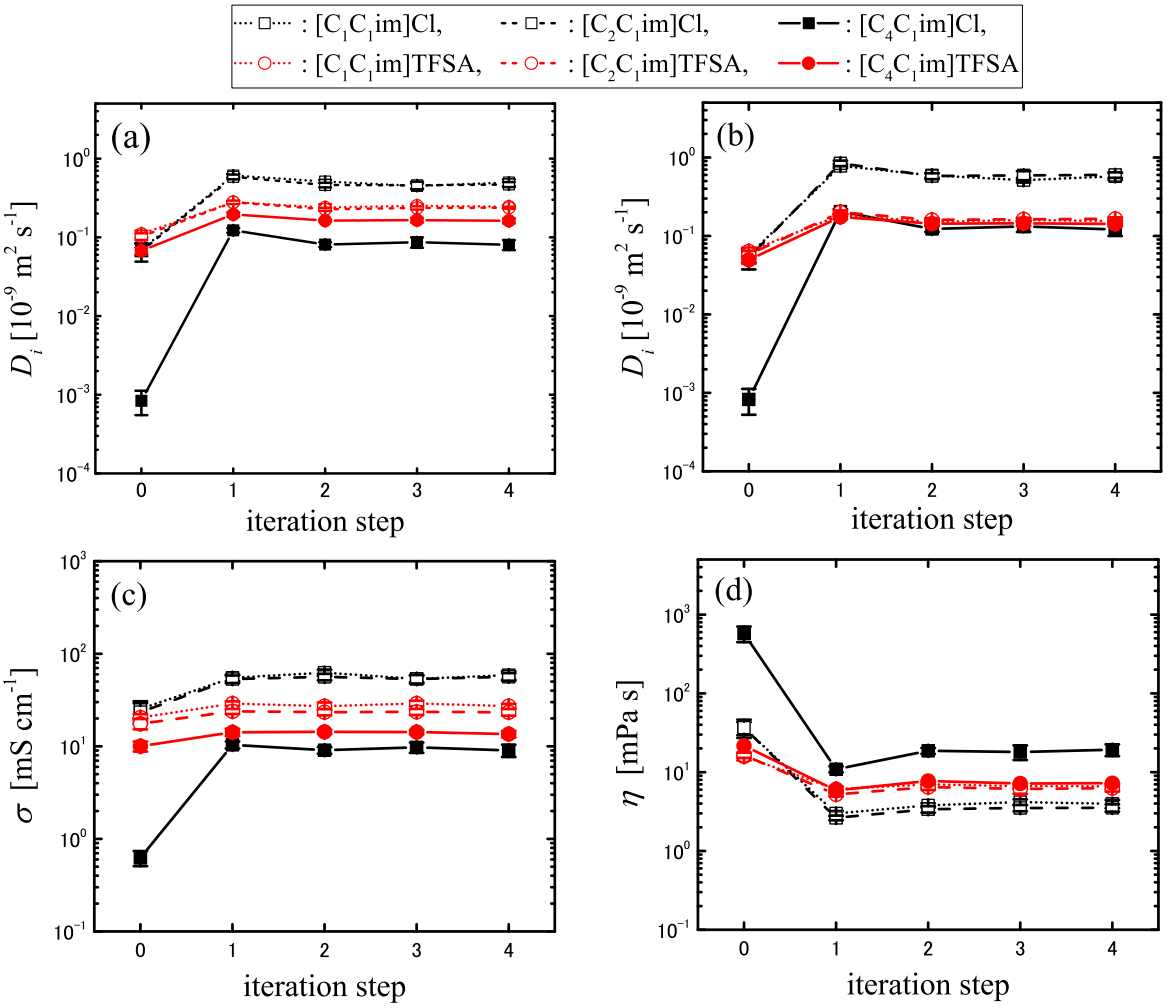

Figure S8: Convergence of the (a) self-diffusion coefficient of cation, (b) self-diffusion coefficient of anion, (c) electrical conductivity, and (d) viscosity through the self-consistent scheme in $[C_1C_1im]Cl$, $[C_2C_1im]Cl$, $[C_4C_1im]Cl$, $[C_1C_1im]TFSA$, $[C_2C_1im]TFSA$, and $[C_4C_1im]TFSA$. All the data are obtained at the reference state listed in Table 1 with the NVT ensemble. Error bars are provided with the standard deviation over the 10 production runs of 100 ns.

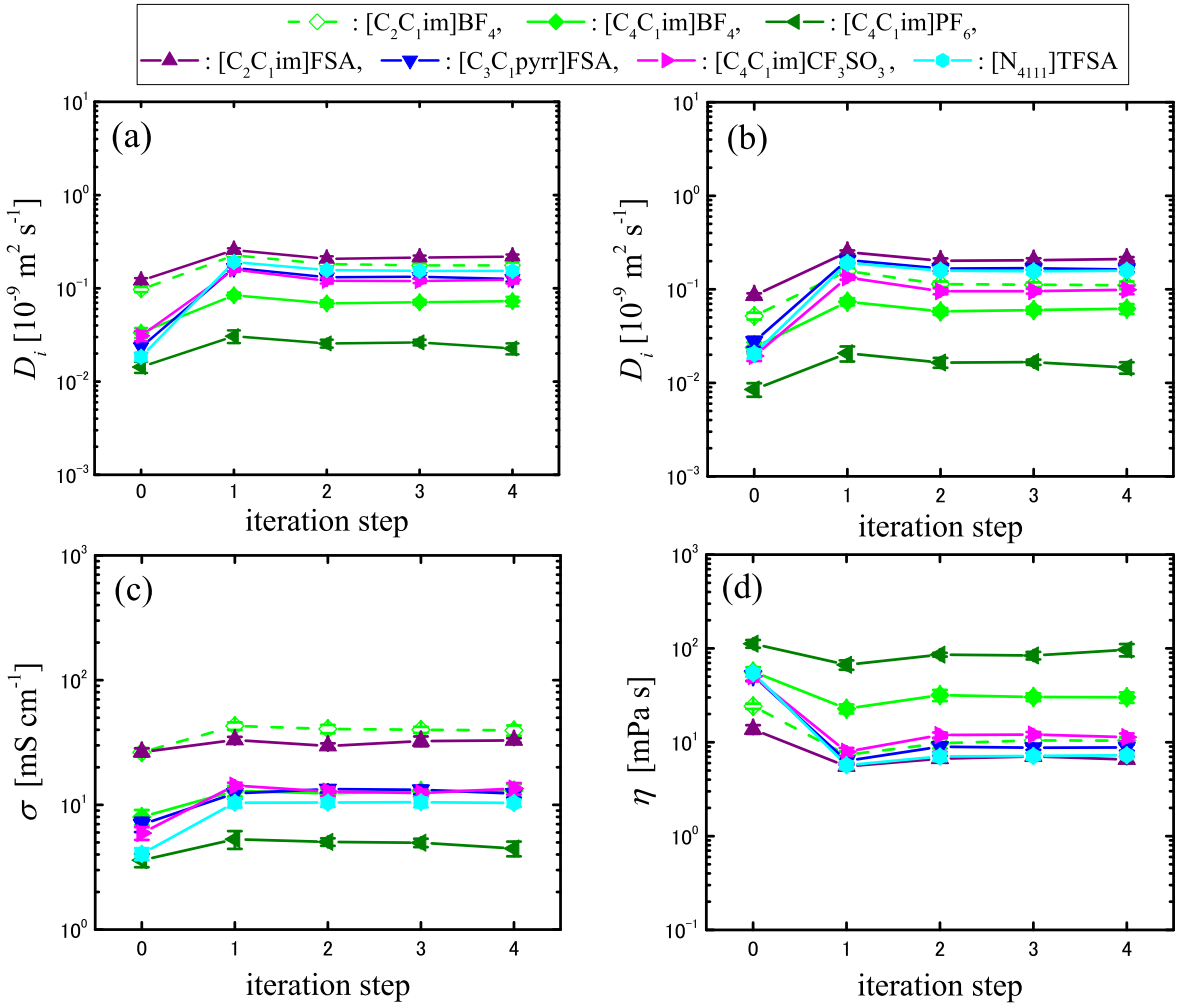

Figure S9: Convergence of the (a) self-diffusion coefficient of cation, (b) self-diffusion coefficient of anion, (c) electrical conductivity, and (d) viscosity through the self-consistent scheme in $[C_2C_1im]BF_4$, $[C_4C_1im]BF_4$, $[C_4C_1im]PF_6$, $[C_2C_1im]FSA$, $[C_3C_1pyrr]FSA$, $[C_4C_1im]CF_3SO_3$, and $[N_{4111}]TFSA$. All the data are obtained at the reference state listed in Table 1 with the NVT ensemble. Error bars are provided with the standard deviation over the 10 production runs of 100 ns.

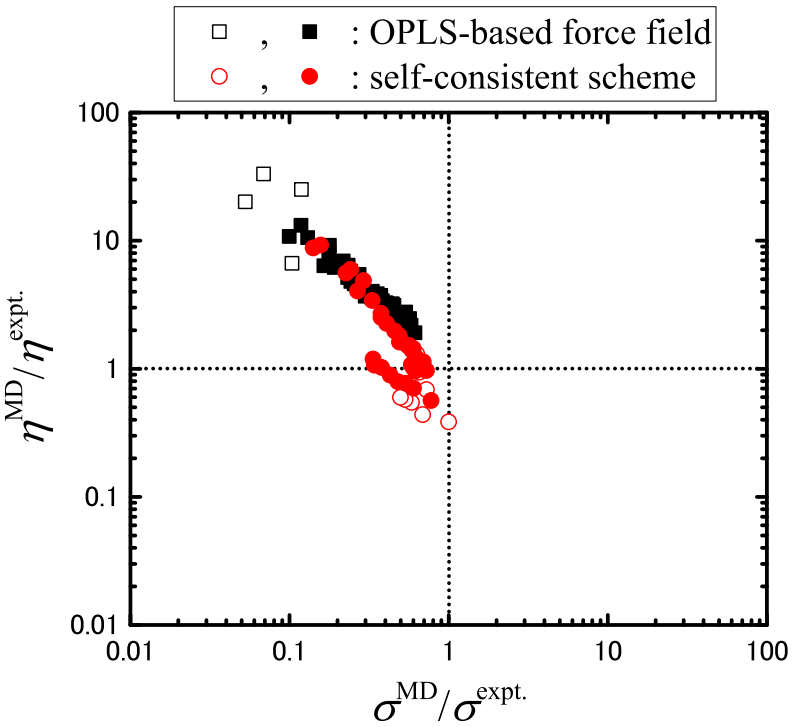

Figure S10: Correlation relationship between the accuracies of calculated electrical conductivity and viscosity obtained with the OPLS-based force field (initial iteration step) and the self-consistent scheme (final iteration step). The calculated properties are compared with the available experimental data. All the data are obtained at the thermodynamic states listed in Table 1 with the NVT ensemble, and are plotted with open symbols for the systems with Cl anion and with filled symbols for the other systems. Dotted lines are guides to the eye for $\sigma^{\mathrm{MD}} = \sigma^{\mathrm{expt.}}$ or $\eta^{\mathrm{MD}} = \eta^{\mathrm{expt.}}$.

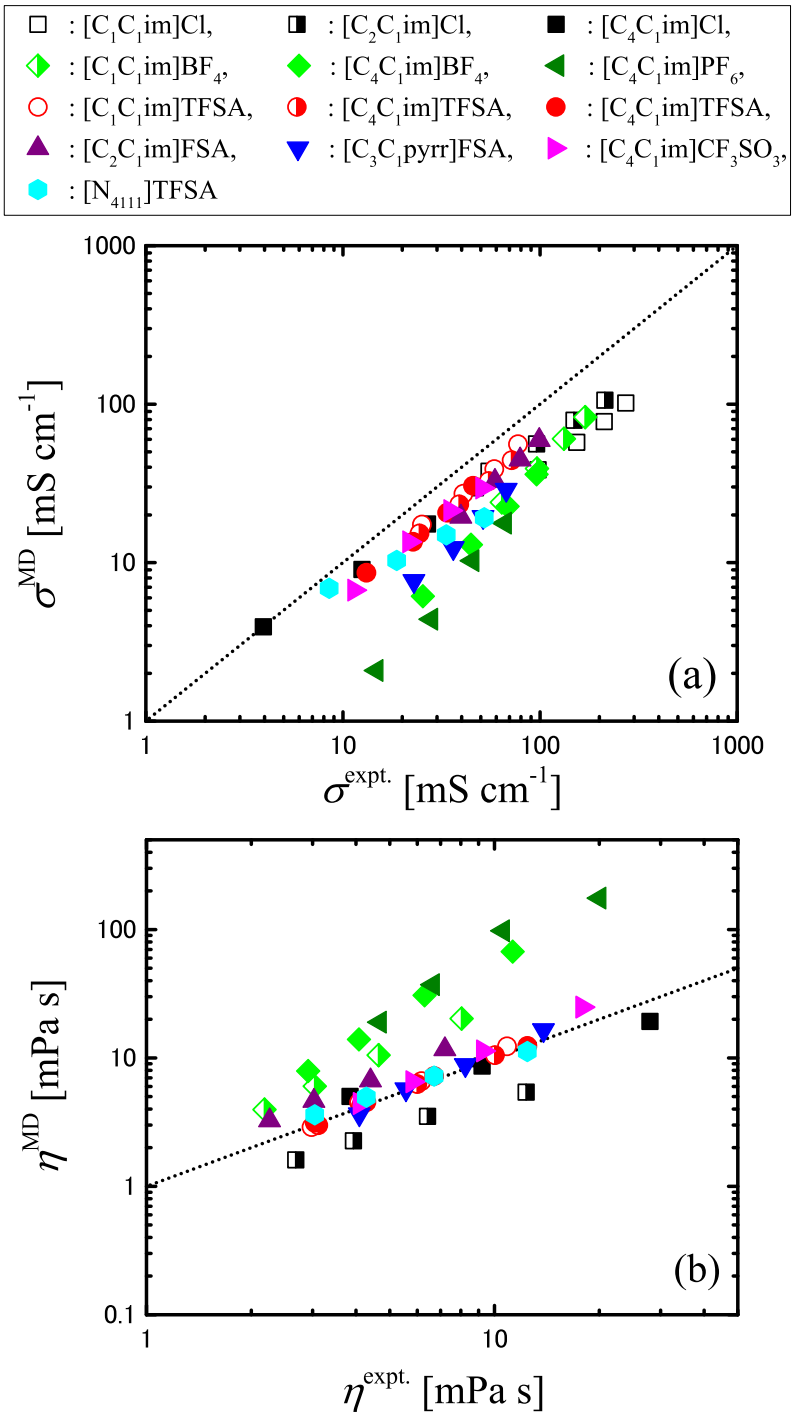

Figure S11: Accuracies of (a) calculated electrical conductity and (b) viscosity obtained with the self-consistent scheme. The calculated properties are compared with the available experimental data. All the data are obtained at the thermodynamic states listed in Table 1 with the NVT ensemble, and σ and η are larger at higher temepratures among the same symbols referring to the identical species. Dotted lines are guides to the eye for $\sigma^{\mathrm{MD}} = \sigma^{\mathrm{expt.}}$ or $\eta^{\mathrm{MD}} = \eta^{\mathrm{expt.}}$.